Experimental and DFT Approach on the Determination of Natural Gas Hydrate Equilibrium with the use of Excess N_2 and Choline-Chloride Ionic Liquid as an Inhibitor

Mohammad Tariq[1ξ], Mert Atilhan[1*] and Majeda Khraisheh[1*]
Enas Othman[2ξ] and Marcelo Castier[2*]
Gregorio García[3] and Santiago Aparicio[3]
Bahman Tohidi[4]

*Corresponding authors (mert.atilhan@qu.edu.qa ; m.khraisheh@qu.edu.qa; maercelo.castier@qatar.tamu.edu)
ξ Equal contribution

[1]Department of Chemical Engineering, Qatar University
[2]Chemical Engineering Department, Texas A&M University at Qatar
[3]Department of Chemistry, University of Burgos, Spain
[4]Institute of Petroleum Engineering, Heriot Watt-University, United Kingdom

Abstract. This work presents characterization of hydrate forming conditions of a Qatari natural gas type mixture, QNG-S1 obtained using two different experimental methods namely: a bench top reactor and a gas hydrate autoclave (GHA). The obtained experimental results were found in agreement to each other. Another mixture where the QNG-S1 sample was diluted with nitrogen (N_2) in a 1:1 ratio was also characterized for hydrate dissociation conditions using rocking cell apparatus only. The thermodynamic hydrate inhibition effect of a biocompatible ionic liquid, choline chloride (ChCl) has been tested for both QNG-S1 and QNG-S1+N_2 at two concentrations (1 and 5 wt%) using rocking cell apparatus. It has been found thatthe ChCl is showing a typical classical thermodynamic inhibitor behavior for both the tested mixtures QNG-S1 and QNG-S1+N_2 by shifting the hydrate equilibrium towards lower temperature and higher pressure. Likewise, the interaction between ChCl and model hydrate cages was analyzed using Density Functional Theory for characterizing the ionic liquid inhibition mechanism at nanoscopic level.

Keywords: Gas hydrates, ionic liquids, inhibitors, DFT

1. Introduction

Gas hydrates are ice-like crystalline structures where gas components such as methane, carbon dioxide and ethane named as guest molecules are entrapped into the cavities formed by hydrogen bonded network of water.[1-3] Whenever a system of natural gas and water exists at specific conditions of low temperature and high pressure, it is expected that hydrates will form. These conditions often exist during gas processing thereby gas hydrates are serious problem for oil and gas industry.[4,5] The vast development in deep water activities carried out in many locations globally including Qatar, flow assurance has become one of the critically important challenges in overcoming hydrates problem.[6] The formation of stable gas hydrates in the production and transmission pipelines in oil and gas industries can cause operational and safety hazards, as well as production and massive economical loss.[7]

Qatar holds the world's third-largest proven reserves of natural gas at 885 trillion cubic feet. Because of its desert climate, gas hydrate formation may seem an unlikely event in Qatar. However, its natural gas reservoirs are located 80 km offshore and the production of liquefied natural gas (LNG) depends on reliable flow from offshore wellheads to onshore processing facilities. Classical methods for inhibiting hydrate formation are used in order to prevent pipeline plugging but changing gas concentrations and operating conditions make flow assurance challenging in the North Field from both economically and processing perspectives.[8]

Generally, industries avoid hydrate formation by injecting thermodynamic inhibitors (THIs), commonly methanol and mono-ethylene glycol, which create unfavorable conditions for hydrate formation.[6,9-11] However, due to the reported health, safety, and environmental concerns that have been affiliated with the use of THIs, an alternative class known as low dosage hydrate inhibitors (LDHIs) have been developed in the recent years and have been used in the field of flow assurance and gas hydrate mitigation in both oil and gas pipelines.[6,12,13] A new class of novel environmentally friendly inhibitors, known as ionic liquids (ILs) have recently caught the attention of researchers but still there are several critical issues which needs to be addressed for their implementation as a promising solution for hydrate inhibition as discussed in a recent review by Tariq et al.[14] Most of the ILs tested so far for hydrate inhibition belongs to imidazolium cation based family, which is known to be toxic.[15] Thus, it is advisable to test ILs, which are non-toxic and biodegradable for hydrate inhibition purposes. The tunable nature of ILs allows us to design them as environmentally friendly compounds by carefully selecting the

cation/anion combinations. In the current work, we have used one such compound known as 2-hydroxy-N,N,N-trimethylethnnminium chloride, also known as choline chloride (ChCl), which belongs to environmental benign and bio-compatible class of IL.[15]

Nitrogen rich gas mixtures are available in considerable amounts in many parts of the world such as: California Great Valley (USA), the Volga-Ural basin (Russia), the Yinggehai basin (China), the Central European basin (Northern Germany and Western Poland) and many more.[16] These nitrogen rich natural gases contain N_2 in approx. 10 – 85 vol% concentrations. These mixtures are being used either as pipeline quality fuel by upgrading them through N_2 removal or used directly as low quality fuel or an additive in certain amount to the high CH_4 gas network.[17]

It is interesting to note that in a recent work, Obanijesu et al.[18] reported that the presence of N_2 and/or H_2 in specific conditions act as hydrate inhibitor for natural gas in pipelines. Although N_2 is a hydrate former itself but the pressure and temperature (P,T) conditions required for hydrate formation are relatively high (in the temperature range of -1 to 13.2 $^{\circ}$C for 144 to 554.2 bars pressure region) compared to hydrocarbons.[19] The idea is very interesting given the fact that nitrogen is relatively economical and requires less sophisticated infrastructure as compared to flammable chemical inhibitors like methanol. This study encourages us also to test the reported theory by measuring the hydrate forming conditions in a natural gas sample, which is rich in nitrogen and its comparison to undiluted sample. Effect of ChCl inhibitor on both the samples was also observed.

Thus the objectives of this work are manifold: (i) It presents the investigation on the hydrate formation/dissociation conditions in a synthetic multi-component gas mixture whose composition is typical of a Qatari natural gas (Table 1) and another sample mixture diluted to half of its composition with N_2 referred as QNG-S1 and QNG-S1+N_2, respectively. (ii) ChCl ionic liquid at two percentages (1 wt% and 5 wt%) was tested for its hydrate inhibition efficiency for both the gas mixtures (QNG-S1 and QNG-S1+N_2) using rocking cell apparatus. (iii) Moreover, to unravel the mechanism of hydrate formation, dissociation and inhibition in both QNG-S1 and QNG-S1+N_2 systems the borescope camera images installed in gas hydrate autoclave have been used and (iv) The characterization of the effect of ChCl on hydrates structure is analyzed at nanoscopic level using Density Functional Theory (DFT). Thus, this study will complete the first detailed characterization of hydrate forming conditions for Qatari

natural gas type mixture, its nitrogen rich version, gas hydrate inhibition performance of a biocompatible ionic liquid and possibility of N_2 in acting as hydrate inhibitor.

2. Experimental and theoretical methods

2.1. Materials. The sample of synthetic Qatar Natural Gas type mixture (QNG-S1) was procured from Quality Specialty Gases, Qatar with a stated mixtures composition accuracy of ±2%. Details about the various components and their relative uncertainty are furnished in Table 1. Nitrogen was purchased from Buzware Scientific and Technical Gases, Qatar, with a stated purity of 99.9%. Choline Chloride with a stated purity of ≥99% has been purchased from Iolitec. Throughout the experiments Millipore Quality water has been used for making solutions. All the IL inhibitor solutions were prepared by weighing on an electronic balance with a precision of ±0.00001 g.

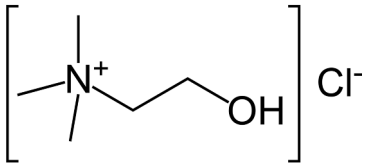

Scheme 1: Structure of (2-hydroxyethyl)trimethylammonium chloride or Choline Chloride (ChCl).

2.2. Experimental methods. Micro bench top reactor (Parr, USA), gas hydrate autoclave and rocking cell apparatuses (both from PSL Systemtechnik, Germany)have been calibrated using grade methane and ultra-pure-grade carbon dioxide gases with known HLVE data to check their performances and validation. Then, QNG-S1mixture was tested alone and in presence of various concentration of hydrate inhibitor to obtain HLVE data. Isochoric pressure search method[22] has been used to get the hydrate liquid-vapor equilibrium data in all the apparatuses.

2.2.1. ***Micro bench top reactor.*** The high pressure Parr reactor with an internal volume of 600 ml was modified for the experiments by adding a whisk like stirrer and removal of internal cooling coil and dip tube. The reactor was filled with 180 ml water and the headspace of the reactor was then purged with a gas composition employed to form gas hydrates. The reactor was sealed and pressurized to the desired pressure with the gas mixture. The pressure of the reactor was maintained and the contents mixed with a high rate of stirring for 2 hours. The reactor was

placed in a cooling bath set to 20 °C. After this equilibration stage, the reactor was re-pressurized to the same pressure, sealed completely, and the stirring rate reduced. The automated computer interface was enabled, and the data logger was set to collect temperature, pressure and torque measurements every 2 seconds. The temperature of the reactor was held at 20 °C for an additional hour. The automated chiller program was then initiated to cool the reactor down to 2 °C. The reactor was held at the final temperature of 2°C, for 24 hours. The reactor was the warmed back to 20 °C (at a rate of 0.1°C per minute) and maintained there for few hours.

2.2.2. ***Gas hydrate autoclave.*** The high-pressure autoclave cell (PSL Systemtechnik, Germany) having a total volume of 400 ml can withstand pressure upto 200 bars. Autoclave lid and all mounted head connections such as borescope-camera, temperature/pressure sensors and inlet/outlet gas valves were detached from the vessel after discharging any internal pressure via opening the gas release valve. The magnet housing of the autoclave was washed carefully several times from inside with distilled water and filled with 135 ml of the aqueous solution to be studied (i.e., water with/without inhibitors). Lid thread was also cleaned from foreign particles and well-greased with the lubricant. Then the magnet housing was sealed properly through mounting the head connections and carefully closing the lid by hand. The aqueous content within the vessel was flushed twice by purging it with the tested gas up to the full bottle pressure to ensure that the vessel didn't have any gas impurities. The vessel was charged with the tested sample of QNG up to 60 bar (bottle maximum pressure) and in order to reach the desired/started pressure the system was connected to a high pressure generator, which is a manually operated piston screw pump used to compress the tested gas within a small volume to develop high pressure (i.e., up to 650 bar). Temperature/pressure conditions within the cell were monitored via display of Hydrate software until they were stabilized. Hydrate software main window was opened to design the whole experimental protocol. The script was edited depending on isothermal cooling method according to following steps (a) initialization phase of the experiment was started to adjust autoclave temperature to 20 $^{\circ}$C (start temperature) and to make an overall check for experiment - mainly cell leakage. This was completed with fast stirring (500 rpm) in order to equilibrate and saturate liquid/gas mixture. (b) The experimental phase of the experiment was then started by cooling the fluid inside the vessel rapidly with rate (1.8 $^{\circ}$C/hr) from 20^{o}C to 2°C with agitation (150 rpm), then the system was left for two days (48 hours) at

2°C to form hydrate. By the time hydrates were formed, stirrer was stopped, as it plugged the cell. In autoclave, gas mixture took longer time to form hydrate plug, this is mainly due to its large volume 400 ml compared to bench top reactor 100 ml. (c) After hydrate was formed, heating process was started back to the initial temperature with tremendously slow rate (0.18 °C/hr) for complete hydrate melting. Step-wise heating method was used during the hydrate dissociation period and 12 hours of intermission has been given at every 12 hours for the experiments. This makes approximately heating rate of 1.44 °C per day. However, in a recent work, Semenov et al.[20] have reported that up to a certain range (0.5 K/hr) heating rate does not affect the determination of equilibrium dissociation point of methane and argon hydrates using the rocking cell assembly. We have provided some P-T loops (Fig. 2 of Supporting Information) showing the absence of any metastability issue using the aforementioned heating rate. While the script is running, pressure, temperature and time can be monitored in the main window of data acquiring software.

2.2.3. ***Rocking Cell assembly.*** The rocking rig assembly (PSL Systemtechnik, Germany), Figures 1 and 2, used in this study contains five test cells. This means that five runs can be performed simultaneously. However, the only variables possible, for these simultaneous runs, can be the composition of the sample and pressure. To start a fresh experiment the test cell was removed from its platform axis after it was depressurized and the temperature sensor and pressure supply tube were disconnected. Then it was mounted on the assembling aid and the screw lid was opened with a jaw wrench. The ball casing of the test cell and the mixing ball were washed carefully for several times with distilled water, ethanol and dried then filled with the prepared test mixture (i.e., ultrapure water and inhibitors) according to the experimental requirement. Then the test cell was sealed properly in the same way it was opened, reinstalled to its corresponding place on the platform axis in RC5 bath, and reconnected to the temperature sensor and pressure supply. The test procedure with this experimental set-up was started with filling each cell (with maximum volume of 40 cm^3) with 15 ml of ultrapure water, then pressurized it directly with the sample gas QNG-S1 to the target pressure, as desired by each set of the experiments.

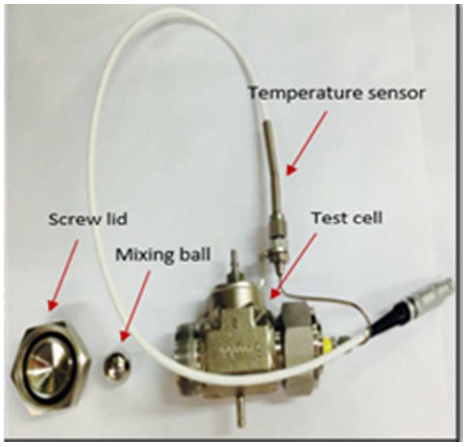

Figure 1. A typical opened up rocking rig assembly test cell after detachment from the mounting.

Each test cell with its aqueous content was flushed, filled with tested sample of QNG-S1 and pressurized up to the desired/started pressure following the same manner applied in high pressure autoclave vessel. After temperature/pressure conditions within the each test cell were stabilized, RC-5 software was started to design the whole experimental protocol. The script was edited depending on isothermal cooling method following the same initialization and experimental phases applied in autoclave except the hold time required forming hydrate plug and the way of creating turbulence and agitation. Liquid vapor mixture within each cell was left for 24 hour at 2 $^{\circ}$C after it was cooled from 20 $^{\circ}$C, half the time required for the same mixture within autoclave. This is mainly due to its small volume (40 ml) compared to autoclave (400 ml). Moreover the mixing module was programmed according to the following parameter: Rocking rate: 10 rocks/ min, Rocking angle: 30$^{o.}$ While the script is running, pressure, temperature and time data can be monitored in RC-5 main window. Further details on rocking cell assembly can be found elsewhere.[23-25]

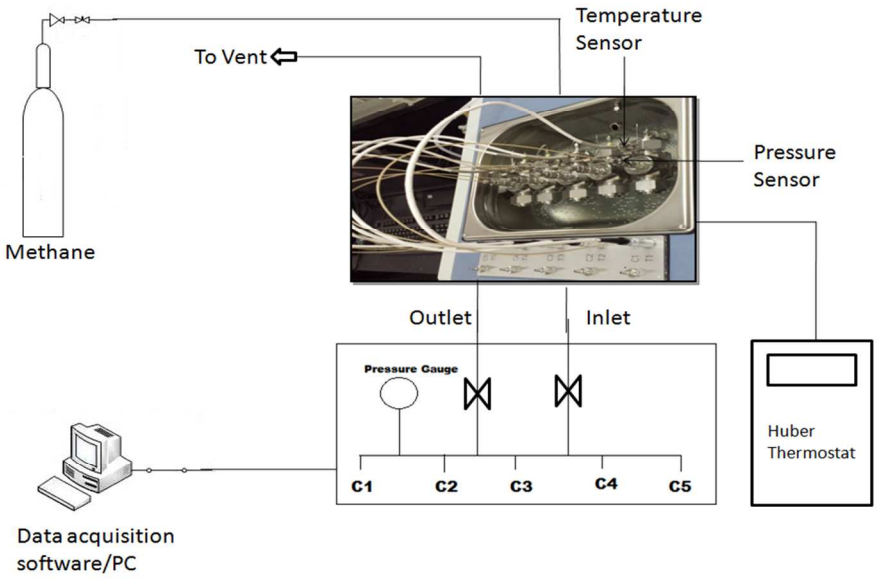

Figure 2. Schematic diagram of the rocking cell (RC-5) assembly.

2.2.4. ***Preparation of diluted sample of Qatar Natural Gas type mixture with N_2.*** The nitrogen mixing was carried out both in autoclave and rocking cell apparatuses. In order to do so, first the cells of both autoclave and RC-5 were filled with the QNG-S1 mixture up to the maximum bottle pressure (60 bars). Later both the apparatuses were connected to a high pressure nitrogen cylinder having a pressure of 200 bars. Using the high pressure regulator the nitrogen was released into the cells until the pressure within each cell of autoclave and RC-5 reached to 120 bars. The mixture was the mixed properly with stirring and the new composition calculated using the precise pressure and temperature readings from the software windows.

2.3. Theoretical methods. Theoretical study through DFT simulations on the interaction mechanism between ChCl IL and hydrate cages is divided in two sections: i) analysis of isolated IL-hydrate cage systems and ii) analysis of the interactions between one ionic pair and small hydrate clusters. As starting point, DFT simulations were focussed on 5^{12} and $5^{12}6^2$ water cages (with single occupancy), with methane (CH_4) was selected as guest molecule. Then, system composed by one isolated molecule (*i.e.*, choline cation, chloride anion and CH_4), ChCl ionic liquid, both host-guest systems ($CH_4@5^{12}$ and $CH_4@5^{12}6^2$) as well as IL-$CH_4@5^{12}$ and IL-$CH_4@5^{12}6^2$ systems were optimized. For IL-hydrate systems, different relative dispositions

between the ionic liquid and the hydrate were essayed as starting points for the optimizations, focusing our attention on the dispositions of minimal energy. Optimized minima were checked through their vibrational frequencies. In addition, empty 5^{12} and $5^{12}6^2$ water cages were also optimized.

Previous results dealing with DFT simulations on hydrate systems showed the need of including dispersion terms in the selected functional for obtaining reliable results.[26,27] The importance of including dispersion corrections in the applied functional for a correct description of host-guest interactions was previously reported.[28] In a previous work, the interaction energies were calculated using B97D functional,[29] which led to reliable results for hydrates systems,[30,31] with no remarkable errors regarding to MP2 calculations.[28] It is also well known that a remarkable accuracy has been achieved by hybrid functional.[32] On the other hand, ωB97X has shown improved accuracy in thermochemistry, kinetic and non covalent interactions than common (hybrid) density functional.[33] This functional could be defined as the long range corrected (LC) version of B97 functional, which contains a small fraction of the short range HF exchange, as well as long range corrections. Hence, in this work, all optimizations were done at ωB97XD/6-311+G(d,p) theoretical level. ωB97XD functional is a re-optimization of ωB97X functional to include dispersion correction according to D2-approach, with satisfactory accuracy for non-covalent interactions.[34] In our opinion, ωB97XD would be an adequate functional to describe both host-guest interactions as well as IL-hydrate ones. Energies computed in this first approximation were corrected according to counterpoise method to avoid basis set superposition error.[35] All these calculation were carried out using Gaussian 09 (Revision D.01) package.[36]

In a second approximation, systems composed by one ionic pair + hydrate clusters were studied. For this purpose, a small cluster of 218 atoms taken from the crystal structure was selected as hydrate model. Firstly, we selected a DFT method (together with the basis set) able to carry out the required simulations with a moderate computational cost. After several attempts over the model cluster, geometry optimization carried out a PBE/DZP[37] theoretical level as implemented in SIESTA 3.2 package[38] provided the best compromise between optimized structures (in comparison with experimental ones) and computational cost. Then, systems composed by one ionic pair and the hydrate cluster were optimized at this level. For IL-cluster systems, different relative disposition between the ionic liquid and the hydrate cluster were used as starting points for the optimizations, which were obtained placing the IL over different regions

of the model cluster. Based on the optimized structures (some of them led to the same optimized structure), single point calculations were performed at ωB97X-D3/6-311+G(d,p)[39] theoretical level as implemented in ORCA package,[40] and molecular properties computed at this level were used for the discussion.

3. Results and Discussion

3.1. QNG-S1 gas hydrate phase characterization. It can be inferred from Table 1 that the synthetic mixture of QNG-S1 is a complex one containing several hydrate promoters and inhibitors. The mixture is rich in methane up to 85% (in moles) with presence of many other hydrate formers such as CO_2, C_2H_6, C_3H_8 and N_2 where these individual components's hydrate forming conditions differ from each other. Gas compositions were checked with GCMS for the the uncertainties and are in agreement with the ones provided by the vendor. It is expected that there will be formation of several/complex crystals in the system given the fact that the components differ in size and nucleation conditions also differ for individual component. Hydrate simulator software HydraFLASH[21] predicts that the QNG-S1 mixture will form type II hydrates that assert the previous assumption. Moreover, the borescope camera images are also indicative of this phenomenon (Section 3.5). Reproducibility of the measurements has been conducted for the validation of the measurement points. Methane + water system has been measured repeatedly by using all the above-mentioned apparatus and no significant effect has been observed. Moreover, the values of hydrate dissociation points obtained for methane agree well with the values reported in the literature, which validate the apparatus for this study (Fig. 1 Supporting Information).

Table 1 shows the relative uncertainties in various components, which will directly affect the global composition of the QNG-S1. These large uncertainties were reflected in the experimentally obtained values using different apparatuses. It must be stressed here that the prime objective of this work is to provide the evidence of hydrate formation in the complex gas mixture of QNG-S1 which has never been reported before. The strategy to mitigate the QNG-S1 hydrates using ChCl and/or N_2 dilution is another important aspect of this work.

Table 1. Composition of Qatari Natural Gas type mixture (QNG-S1) and relative uncertainties as claimed by the suppliers.

Component	Composition in mol %
methane	0.84990
ethane	0.05529
propane	0.02008
iso-butane	0.00401
n-butane	0.00585
iso-pentane	0.00169
n pentane	0.00147
n octane	0.00152
toluene	0.00090
methyl cyclopentane	0.00102
nitrogen	0.03496
carbon dioxide	0.02331

* Relative uncertainty for samples: CH_4 0.2%, C_2 to C_4 2.0%, C_5 plus higher 5%, N_2 and CO_2 2%.

For the dilution experiments (next section) N_2 was mixed to the current sample and composition was calculated. The new composition of the QNG-S1 mixture after nitrogen mixing becomes almost equimolar. Such that the mixture is diluted to almost half of its composition and becomes nitrogen rich (0.5QNG-S1:0.5QNG-S1+N_2). It should be emphasized here that N_2 also forms the hydrates but at much extreme (P, T) conditions compared to other hydrate forming components found in the QNG-S1 mixture used in this study.[19]

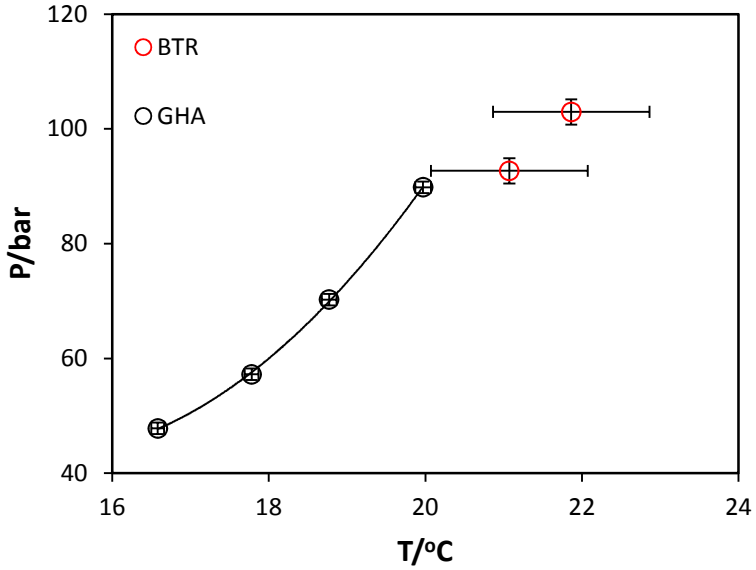

Figure 3. Hydrate vapour-liquid equilibrium curve for Type I Qatari Natural Gas (QNG-S1). Points are experimental data measured from bench top reactor (BTR) and gas hydrate autoclave (GHA). Solid line is guide to the eye.

Figure 3 presents the results of hydrate vapour-liquid equilibrium points of QNG-S1 mixture extracted from the P-T loops obtained from two different experimental apparatuses (Fig 2 Supporting Information). It is evident that although, the results depicted are not in excellent agreement of each other. however, the disagreement between the two experimental apparatuses values is easy to understand since the bench top reactor has poor temperature precision and there are large uncertainties (±2.2 $^{\circ}$C) associated with the thermocouple. QNG-S1 contains almost ~85% methane however compared to methane it is easier to form hydrates in QNG-S1 because of the presence of high molecular weight components in the mixture. This whole scenario suggests that one has to be careful in handling and measurements while dealing with such a complex mixture. Nevertheless, this whole practice proves that QNG-S1 is capable of forming hydrates. Useful data have been collected which might be valuable for the Qatar oil and gas industries to design their flow assurance strategies.

3.2. Choline Chloride as QNG-S1 hydrate inhibitor. It is evident that the choline chloride (Scheme 1) is an ionic liquid from ammonium family, having a structure similar to tetraalkylammonium salts but an additional –OH functional group attached to it. It is showing typical thermodynamic inhibitors characteristics by shifting the hydrate equilibria towards higher pressures and lower temperatures (Figure 4). However, it seems that at higher pressures the effectiveness of 1 wt% ChCl is not as much as at lower pressures. It is also obvious that 5 wt% ChCl is more effective compared to 1 wt% ChCl. The presence of –OH group is very important in order to make hydrogen bonds with 'free water' and shifts the thermodynamic equilibrium through preferential hydrogen bonding.[41,42] These results are encouraging since choline based ILs are mostly biocompatible thus falls into the category of green inhibitors. Although, the inhibition effect is not as great as the conventional ones yet the results pave a way to design more biocompatible ionic liquids which can more strongly participate in hydrogen bonded network of water thereby with enhanced hydrate inhibition effectiveness.[43-45]

Table 2: Experimentally obtained Hydrate dissociation conditions for Qatari Natural Gas (QNG) in absence and presence of ChCl ionic liquid and (ChCl+N_2) as inhibitors.

QNG[a]		**QNG + 1 wt% ChCl**[c]		**QNG + 5 wt% ChCl**[c]	
***T*/°C**	***P*/bar**	***T*/°C**	***P*/bar**	***T*/°C**	***P*/bar**
19.97	89.82	19.00	78.88	19.6	93.76
18.77	70.26	18.00	65.97	18.51	77.73
17.78	57.23	17.00	55.84	16.51	59.62
16.58	47.81	16.00	48.32		
21.07[b]	92.69[b]				
21.86[b]	102.97[b]				
QNG + 1 wt% ChCl+ N_2[c]		**QNG + 5 wt% ChCl+ N_2**[c]		**QNG-S1+ N_2**[c]	
12.64	55.69	13.94	77.56	13.06	59.61
13.77	63.41	16.00	102.96	15.45	82.23
14.61	72.09	16.86	121.61	16.43	98.86
17.57	116.46				

[a]Data obtained using Gas Hydrate Autoclave; [b]Data obtained using bench top reactor; [c]Data obtained using rocking cell apparatus.

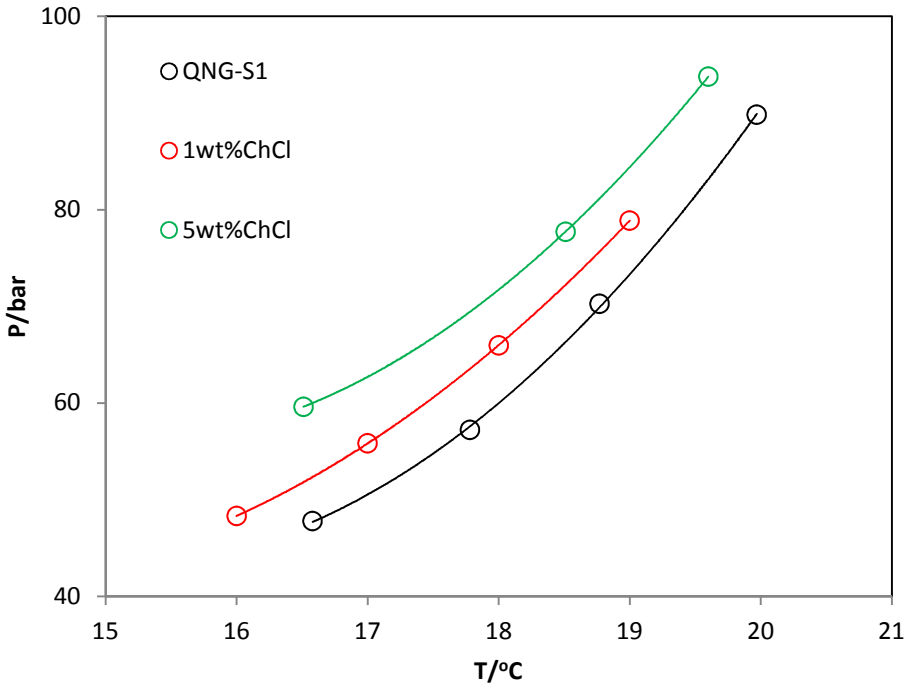

Figure 4. Experimental hydrate vapor-liquid equilibrium curve for Type I Qatari Natural Gas (QNG-S1)obtained using gas hydrate autoclave compared to the curves in presence of 1 and 5 wt% choline chloride obtained using rocking-cell apparatus.

3.3. Choline Chloride as hydrate inhibitor for diluted QNG-S1. As discussed earlier the N_2 has been mixed into the system containing QNG-S1 to form an equimolar N_2 diluted QNG-S1 mixture, QNG-S1+N_2. The mixture was characterized for hydrate dissociating conditions using RC-5 assembly followed by ChCl testing as hydrate inhibitors on this mixture as done previously for QNG-S1. Figure 5 shows the hydrate dissociation curves for QNG-S1, QNG-S1+N_2 alone and also in presence of 1 and 5 wt% ChCl. It can be immediately inferred from the plots that this mixture will form hydrates but at relatively high pressures since it is diluted with N_2, which does form hydrates but at much extreme conditions as stated earlier. The shifting results for the mixture in presence of ChCl are a bit different compared to undiluted QNG-S1. Almost no inhibition effect for 1 wt% ChCl and there is a typical thermodynamic effect for 5 wt% ChCl has been observed. We will further analyze the data in next section to understand the probable cause of these trends.

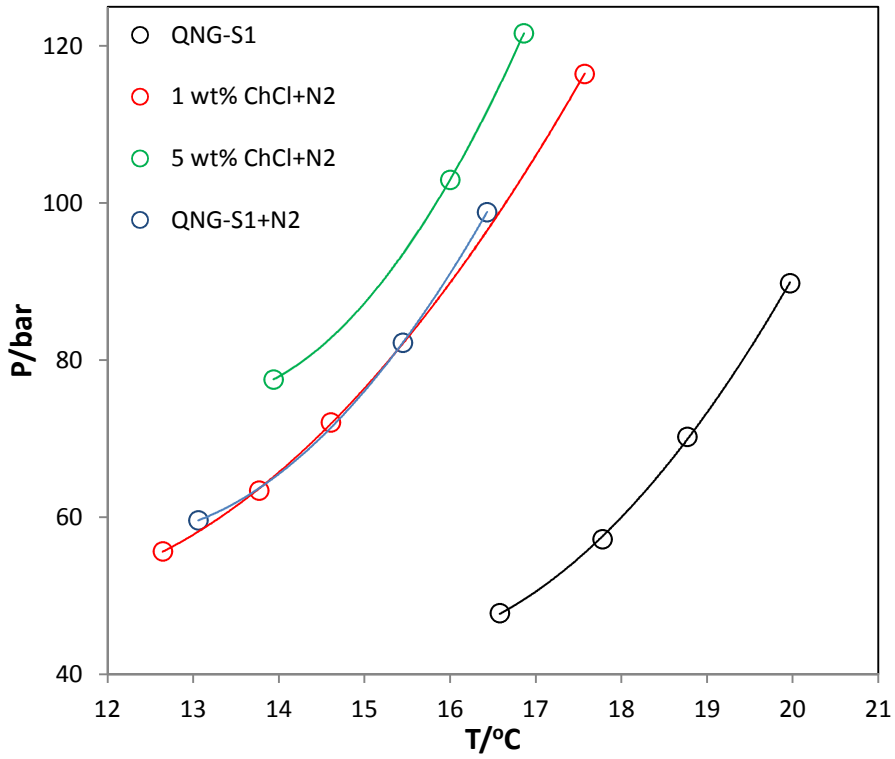

Figure 5. Experimental hydrate vapour-liquid equilibrium curve for Qatari Natural Gas (QNG-S1) obtained using gas hydrate autoclave compared to the curves without/with nitrogen dilution (QNG-S1+N_2) in presence of 1 and 5 wt% ChCl obtained using rocking cell apparatus.

3.4. Analysis of HLVE Data. In this section we have analyzed the HLVE curves by converting them to the trends of hydrate suppression temperatures in presence of ChCl in various concentrations for diluted QNG-S1+N_2 and QNG-S1 alone. The results are depicted in Figure 6 (A-D). Four different conditions arise with all the data set: (*A*) Where the effect of ChCl in different concentrations at QNG-S1 hydrates dissociation conditions is depicted; (*B*) Where the inhibition effect of N_2 on QNG-S1 hydrate forming conditions is shown, also one can translate it into the relatively different conditions required to form the hydrates for this dilute mixture; (*C*) where the combined effectiveness of both (ChCl+N_2) in QNG-S1 hydrate inhibition is considered; and (*D*) When the hydrate inhibition effect of different concentrations of ChCl on the diluted mixture is observed.

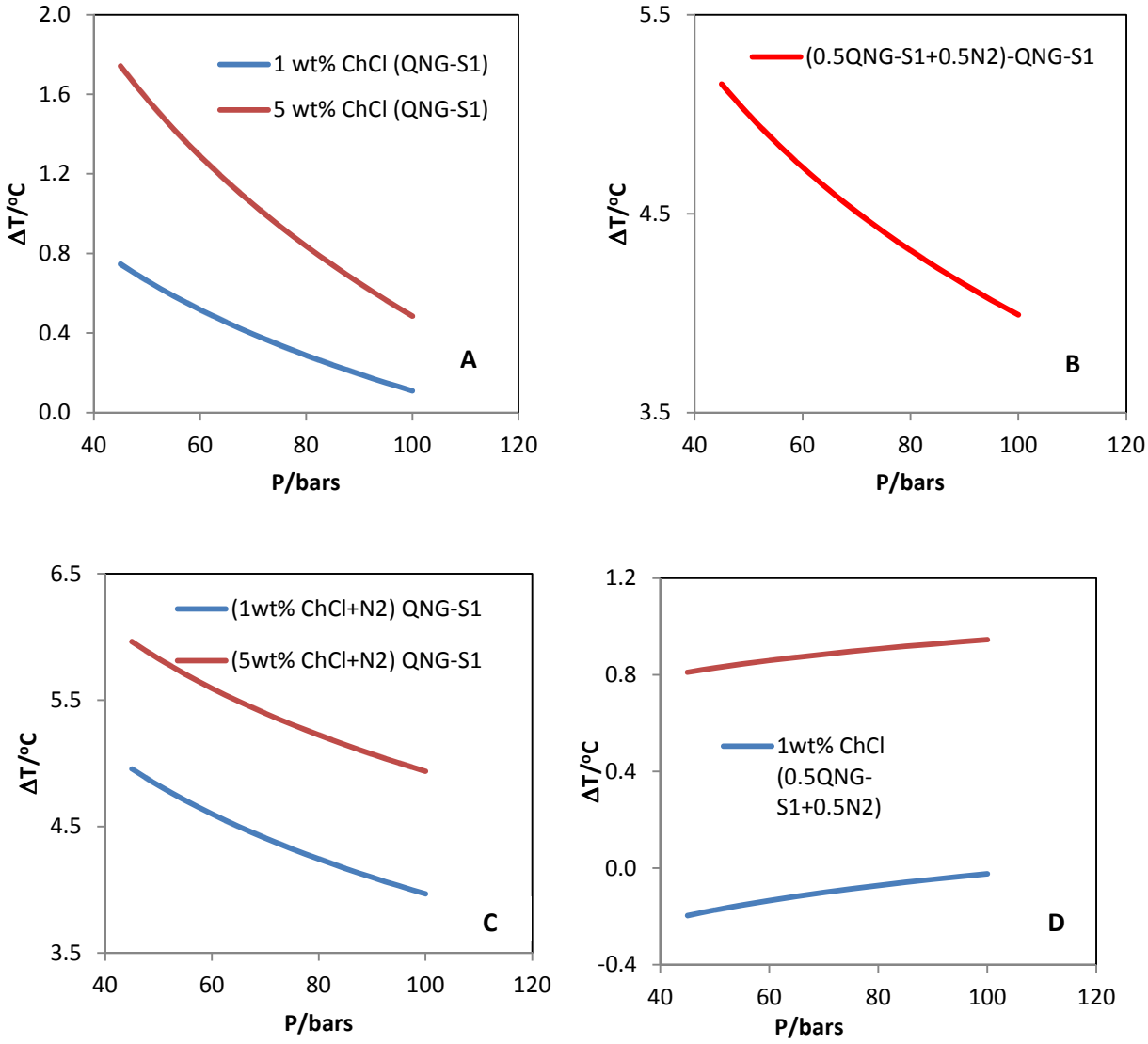

Figure 6. Hydrate suppression temperature as a function of pressure for Qatari Natural Gas hydrates in presence of ChCl (1 and 5 wt%) with/without N_2 purging.

Some important points can be extracted from the trends of hydrate suppression temperature in the above-mentioned four conditions and in presence of various amount/type of inhibitors. At a given pressure in this study ChCl+N_2 are much more effective in shifting the QNG hydrate phase boundaries compared to ChCl alone (Fig. 6 A and C). On the other hand, the magnitude of hydrate suppression temperature caused by ChCl+N_2 is in the range of 5-6 $^{\circ}$C at lower pressures compared to 0.7-1.7 $^{\circ}$C for ChCl in similar pressure range (45-60 bars) compared to almost constant 0.1°C for undiluted QNG-S1 in similar pressure range (Fig. 6 A and C). It is

also observed that at higher pressures (80-100 bars) the magnitude of suppression temperature considerably decreases indicating that with increasing pressure the hydrate inhibition ability of both inhibitor systems deteriorate (Fig. 6 A and C). Moreover, as found in Fig. 4 and 5, the difference between the 1 and 5 wt% ChCl in shifting the hydrate equilibrium is also evident here in terms of ΔT. The difference is smaller for ChCl compared to ChCl+N_2 (Fig. 6 A and C). As can be seen from Fig. 6 B, it is evident that mixing N_2 alone can be an effective strategy for hydrate inhibition. N_2 is showing a suppression temperature of ~5 °C at lower pressures (40-60 bars) and ~4 °C at higher pressures (80-100 bars). Yet, Fig. 6 D reveals that ChCl is not as effective in inhibiting the hydrate formation in the diluted (N2 rich) mixture of QNG-S1 as compared to undiluted QNG-S1. The trends are also reversed with pressure, at lower pressures the ChCl inhibiton is less effective and at higher pressures it is relatively more. For 1 wt% ChCl the data seems a bit puzzling, showing negative values of □T at lower pressures and as the pressure is increasing the magnitude of □T is tending towards positive values. As the magnitude is very small (~0.2) this can be accounted for the uncertainty in calculation of hydrate suppression temperature obtained through fitting the experimental data points. Thus, in our opinion this strange behavior can be neglected given the uncertainty associated with the dilution experiments.

3.5. Borescope Camera Image analysis. In Figure 7 we have presented some of the images for QNG-S1 hydrate formation-dissociation cycle with and without inhibitor. As one can see in the left panel the QNG-S1 without any inhibitor starts forming hydrates at around 270 mins. It can also be referred roughly as induction time and later the crystal growth start taking place until the hydrate blocks the pipeline at around 4410 min. It seems a rock like structure. As indicated previously Hydraflash predicted QNG-S1 hydrates will form a type II crystal structure.

QNG-S1: No Inhibitor	QNG-S1 + N_2 with 1wt% ChCl
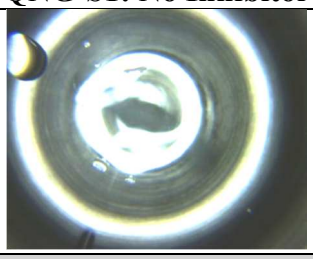	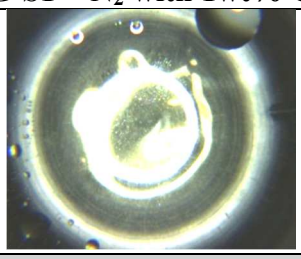
t = 0 *min* (initial mixing)	*t* = 0 *min* (initial mixing)
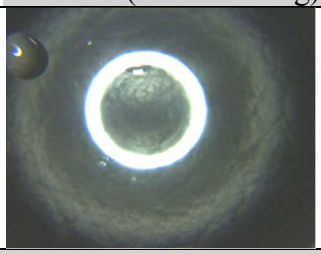	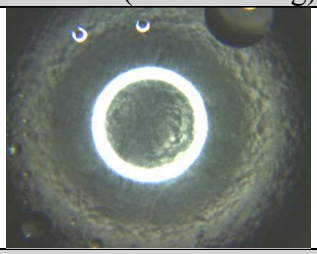
t = 270 *min* (Initial hydrate formation)	*t* = 360 *min* (Initial hydrate formation)
	
t = 4410 *min* (Maximum Hydrates)	*t* = 4410 *min* (Maximum Hydrates)
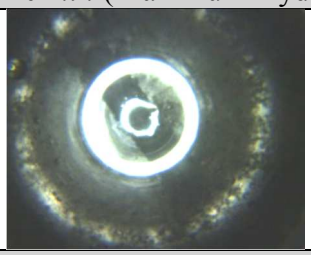	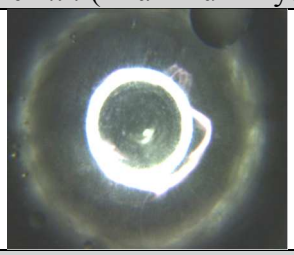
t = 9780 *min* (Hydrates Dissociation)	*t* = 8970 *min* (Hydrates Dissociation)
	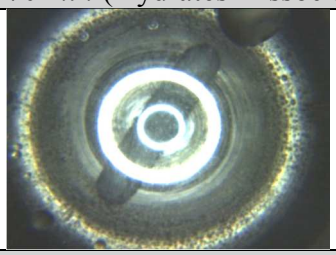
t = 10530 *min* (End of Experiment)	*t* = 10530 *min* (End of Experiment)

Figure 7. Borescope camera images from gas hydrate autoclave (GHA) showing the cycle of Qatari type natural gas hydrate formation and dissociation without any inhibitor (left panel) and in presence of 1 wt% ChCl+N_2 rich environment (right panel) at various time intervals.

Whereas, in the right panel, system contains diluted sample, QNG-S1+N_2 in presence of 1 wt% ChCl is shown. Here the situation is very different compared to the previous one. As one can see the first sign of hydrate formation (induction time) is around 360 min compared to 270 min of QNG-S1 alone. It shows there is a clear delay in hydrate formation in presence of ChCl+/N_2. Later after prolonged time in the experiment the hydrates formed but not as much as in the previous case. Even the formed hydrates at 4410 min (same time frame) doesn't look similar to hydrates of QNG alone. They seem more like slurry or not so strongly associated. This could be due to the reason that ChCl is analogous to quarternary ammonium salts known for their anti-agglomerant characteristics. Another plausible reason for this phenomena could be the presence of N_2 in the system. It also suggests that the ChCl+/N_2 system is a unique option for hydrate inhibition for Qatari natural gas. However, more systematic and detailed studies are needed in order to unravel the mechanism of the inhibition phenomena of this synergistic system.

3.6. DFT Analysis on IL-hydrate interactions. Analysis of IL-hydrate cage systems has been done in terms of geometrical changes on hydrates geometries upon interactions with ChCl ionic liquid, energetic of host/guest system in presence and absence of selected IL. The optimized geometries of $CH_4@5^{12}$ and $CH_4@5^{12}6^2$ cages are shown in Figure 8. In this work, the strength of host-guest interactions has been assessed trough its interaction energy (ΔE^{HG}), which has been defined as:

$$\Delta E^{HG} = E(CH_4@5^{12}) - [E(CH_4) + E(5^{12})] \quad (1)$$

where $E(CH_4@5^{12})$, $E(CH_4)$ and $E(5^{12})$ stand for the energies of $CH_4@5^{12}$, methane molecule and 5^{12} empty cage, respectively. An Analogous expression can be defined for $CH_4@5^{12}6^2$ system. These interaction energies are one key property to characterize clathrate type systems. In this work, interaction energies are -7.27 kcal mol^{-1} and -6.42 kcal mol^{-1} for $CH_4@5^{12}$ and $CH_4@5^{12}6^2$ cages, respectively, at ωB97XD/6-311+G(d,p) theoretical level. These values are in concordance with those previously reported at MP2/6-311++G(d,p) level (-7.78 kcal mol^{-1} and -6.80 kcal mol^{-1}).[28] Small differences point out to the quality of ωB97XD/6-311+G(d,p) level to describe host-guest interactions. More negative energies of $CH_4@5^{12}$ system agrees with the more favoured formation of this cage.[31]

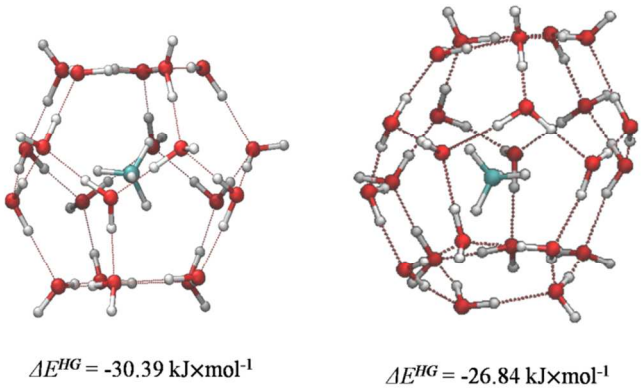

Figure 8. Optimized Structures of $CH_4@5^{12}$ and $CH_4@5^{12}6^2$ cages. Host-guest interaction energies (ΔE^{HG}) of both systems are also included. Red dotted lines stand for water-water H-bonds.

Optimized structures of ChCl interacting with $CH_4@5^{12}$ and $CH_4@5^{12}6^2$ cages are displayed in Figure 9. In both cases, two different arrangements between the IL and the clathrate were found (labelled as I and II / III and IV for 5^{12} / $5^{12}6^2$ cages). For these optimized structures two different interaction energies can be defined. The first one can be used to assess the magnitude of IL··· clathrate interactions ($\Delta E^{IL\text{-}C}$), which has been defined as follow:

$$\Delta E^{IL\text{-}C} = E(\text{IL-CH}_4@5^{12}) - [E(\text{IL}) + E(\text{CH}_4@5^{12})] \quad (2)$$

where $E(\text{IL-CH}_4@5^{12})$ is the energy of the optimized IL-$CH_4@5^{12}$ structure (an analogous expression can be obtained for $CH_4@5^{12}6^2$ cage). The second one measures host-guest interactions (ΔE^{HG}, Eq. 1) taking into account the new arrangement of $CH_4@5^{12}$ system upon interaction with choline chloride ionic liquid. For this, single point calculations were carried out over different filled cages using their coordinated obtained from optimized IL-$CH_4@5^{12}$ and IL-$CH_4@5^{12}6^2$ systems. Estimated $\Delta E^{IL\text{-}C}$ values (Figure 9) of both I and II (IL-$CH_4@5^{12}$) / III and IV (IL-$CH_4@5^{12}6^2$) optimized geometries systems lie between -59.82 kJ×mol^{-1} and or 118.21 ??kJ×mol^{-1} / -162.64 kJ×mol^{-1} and -155.37 kJ×mol^{-1}. IL-cage interaction energies are much higher than host-guest ones obtained in absence of ChCl, which points out that selected ionic liquid strongly interact with both cages. For example, $\Delta E^{IL\text{-}C}$ of structure I (which is the smallest one) is about twice than ΔE^{HG} of $CH_4@5^{12}$. Since, ChCl strongly interact with water molecules breaking the cage, ΔE^{HG} values become less negative, i.e., the cage is much less stable in presence of the ionic liquid. Only for structure I, $\Delta E^{HG} < 0$ are obtained (for $CH_4@5^{12}$, ΔE^{HG} = -5.35 kJ×mol^{-1}), please see Fig. 9. The most important changes upon interaction with ChCl are

noted for structure IV, which yields ΔE^{HG} = 31.73 kJ×mol^{-1}. These high values of ΔE^{HG} point out the possibility that the hydrate structure is broken. An examination of the difference between ΔE^{HG} of both cages in absence of the ionic liquid, as well as ΔE^{HG} and $\Delta E^{IL\text{-}C}$ of structures I-IV shows that lower stability of $CH_4@5^{12}6^2$ allows stronger interaction with ChCl ionic liquid, whereas the hydrate structure would also be more easily opened.

Finally, IL-hydrate interactions have been localized and featured through topological analysis of the electronic density (AIM theory). Although four different critical points can be defined according to AIM theory, we have only focused on bond critical points (BCPs), that fulfill the criteria to be defined as H-bond, related with intermolecular interactions between ChCl ionic liquid and water cage molecules. Thus, cation/anion···cage interactions are also displayed in Figure 9 (black/blue). Aimed at studying all BCPs as a whole, we have analyzed the total electronic density sum over all BCPs ($\sum\rho_{(BCP)}$), In addition, based on involved atoms in each interaction, $\sum\rho_{(BCP)}$ can be decomposed as the sum of contributions from cation/anion···cage interactions (Table 3): $\sum\rho_{(BCP)} = \sum\rho_{(BCP,cat)} + \sum\rho_{(BCP,ani)}$.

Table 3. Total sum of the electronic Density ($\sum\rho_{(BCP)}$) over all, [CH]···[Cl] and ion···cage intermolecular interactions. Units are in a.u.

	ChCl	**IL-$CH_4@5^{12}$**		**IL-$CH_4@5^{12}6^2$**	
		I	**II**	**III**	**IV**
$\sum\rho_{(BCP,IL)}$	0.0330	0.0204	0.0250	0.0195	0.0178
$\sum\rho_{(BCP,ani)}$		0.0346	0.0496	0.0513	0.0571
$\sum\rho_{(BCP,cat)}$		0.0328	0.0400	0.0748	0.1504

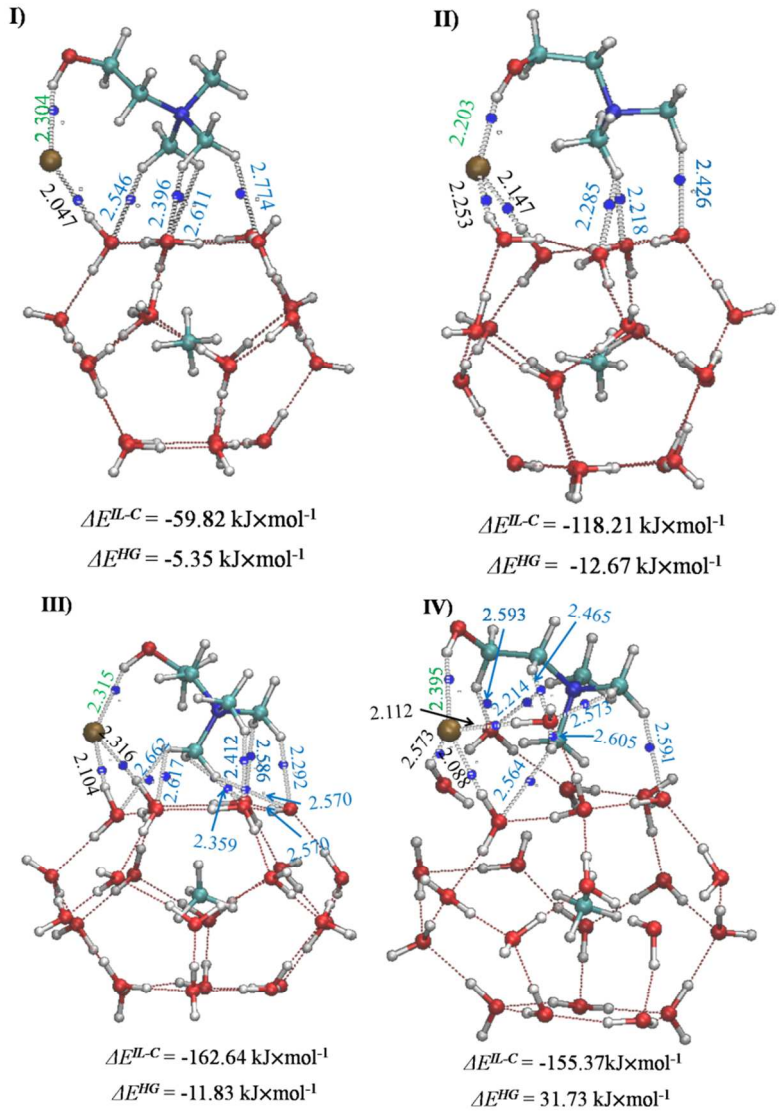

Figure 9. Optimized Structures of IL-CH_4@5^{12} (up) and IL-CH_4@$5^{12}6^2$ (bottom) systems. IL-hydrate interaction energies (ΔE^{IL-C}) and Host-guest interaction energies (ΔE^{HG}) are also shown. Red dotted lines represent water-water H-bonds, while green / black / blue stand for the main [CH]···[Cl] / anion··cage / cation···cage interactions. Only BCP (blue points) corresponds to cation-anion and ion-water intermolecular interactions are shown. Intermolecular bond lengths are in Å.

In addition, the main interaction for ChCl has been also characterized both in presence and absence of hydrate cages (Figure 9 and Table 3). The main interactions between both ions are H-bond between chloride atoms and H of hydroxyl group. Based on our simulations, this H-bond yield a length equal to 2.125 Å and electronic density ρ = 0.0330 a.u. As seen in Figure 9 and Table 3, this H-bond is only scarcely weakened upon hydrate presence. For structure I, a strong H-bond is found between chloride atom and one water molecule, which is the largest

contribution to the $\sum\rho_{(BCP)}$. Nonetheless, there are also four week H-bonds between methyl H and O atoms from water molecules. Although those H-bond yield long lengths ($\simeq$ 2.582 Å) and low electronic density values ($\sum\rho_{(BCP)}$ = 0.0328), they also represent an important contribution to the cage destabilization. Similar trends are noted for the remaining hydrates. Even if, there are two or three clorhide···water cage intermolecular H-bond, while choline···water H-bond provide increasing strengths (lower distances and $\sum\rho_{(BCP)}$ values). These factors agree with ΔE^{HG} and $\Delta E^{IL\text{-}C}$. The most dramatic effects were found in structure IV. As seen in Figure 9, there are three / eight chloride/choline···water H-bonds, which bring out that three water molecules clearly broke the cage arrangement. In fact, the more negative ΔE^{HG} energies are obtained for this structure.

In the second approach a more realistic hydrate model is considered, Figure 10. Regarding to the analysis of the interactions between one ionic pair and small hydrate clusters, Figure 11 draws the optimized structures for the hydrate cluster model (composed by two $CH_4@5^{12}$ plus 2 $CH_4@5^{12}6^2$ cages) interacting with one ionic pair. Aimed at simplify the exposition of obtained results, the analysis of IL-cluster systems has been mainly done based on energy parameters. Thus, binding energy for the interaction between the hydrate cluster and choline chloride ionic liquid has been estimated as (similar than Eq. 2):

$$\Delta E^{IL\text{-}cluster} = E(\text{IL-cluster}) - [E(\text{IL}) + E(\text{cluster})] \quad (3)$$

where E(IL-cluster), and E(cluster) are the energy of the optimized IL-cluster and isolated cluster structures. Destabilization of the hydrate cluster upon interactions with ChCl has been measured as the energy difference ($\Delta E^{cluster}$) between the hydrate cluster in using its geometry in absence ($E(cluster)$) and presence ($E^*(cluster)$) of the ionic liquid, *i.e.*:

$$\Delta E^{cluster} = E^*(\text{cluster}) - E(\text{cluster}) \quad (4)$$

Both $\Delta E^{IL\text{-}cluster}$ and $\Delta E^{cluster}$ paramenter are also displayed in Figure 11, while Figure 12 draws the evolution of both energies for structures V-XII. In general, both approximations yield interactions energies ranged between -60.0 kJ×mol^{-1} and 160.0 kJ×mol^{-1}, with exception structure V ($\Delta E^{IL\text{-}cluster}$ = -17.95 kJ×mol^{-1}). The highest values for interaction energies ($\Delta E^{IL\text{-}cluster}$) between choline chloride ionic liquid and hydrate cluster are obtained for structures VI (-133.40 kJ×mol^{-1}), VIII (-118.22 kJ×mol^{-1}), IX (-124.33 kJ×mol^{-1}) and XII (-153.12 kJ×mol^{-1}). In addition, the strongest interaction between the ionic pair and the hydrate cluster are also related

with the largest destabilization of the hydrate (measured through $\Delta E^{cluster}$). Thus, the largest destabilization are noted for structure XII ($\Delta E^{IL\text{-}cluster}$ = 68.03 kJ×mol^{-1}).

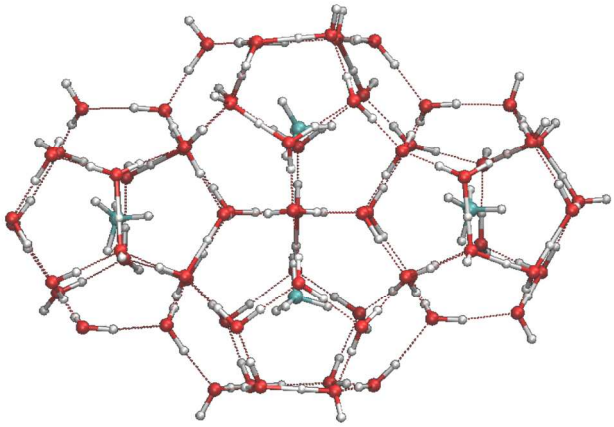

Figure 10. Optimized Structures of hydrate model cluster used in the second part of DFT simulations.

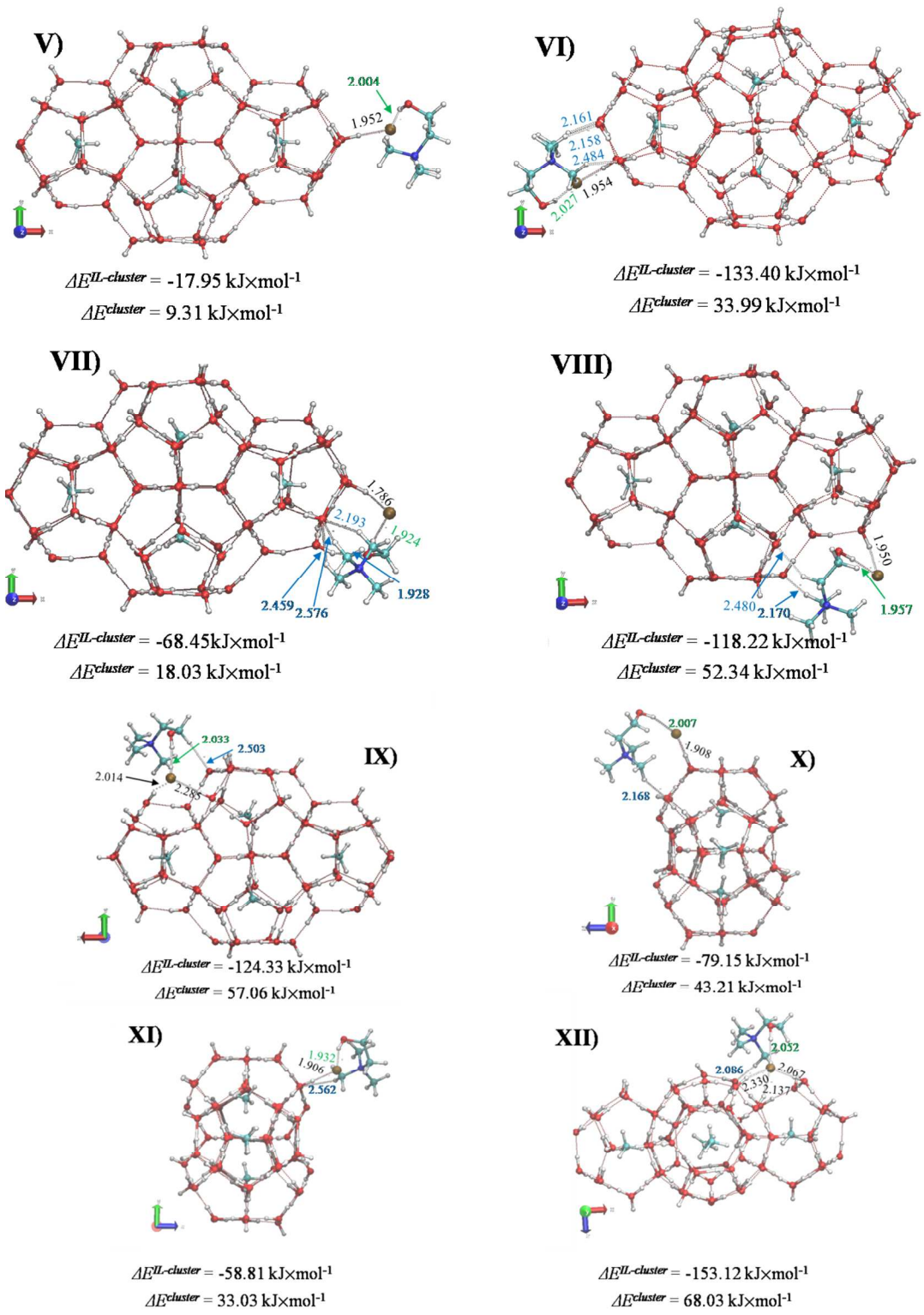

Figure 11. Optimized Structures of IL-cluster showing different relative dispostion between the IL and the cluster. IL-cluster interaction energies ($\Delta E^{IL\text{-}clus}$) and the variation energy of the cluster due to the ionic pair (ΔE^{clus}) are also shown. Red dotted lines represent water-water H-bonds, while green / black / blue stand for the main [CH]···[Cl] / anion··cluster / cation···cluster interactions. Intermolecular bond lengths are in Å.

Figure 12. Computed IL-cluster interaction energies ($\Delta E^{IL\text{-}clus}$) and variation energy of the cluster due to the ionic pair (ΔE^{clus}).

The interaction mechanism has been inferred from the molecular disposition between ChCl regarding the hydrate. As seen in Figure 11, choline chloride ionic pair is interacting with one face of cage 5^{12}, where the main interaction is taking place between the chloride anion. This interaction mechanism is similar to those described for structures I and II. Nonetheless, in structures VIII, IX and XII the ionic pair is simultaneously interacting with both 5^{12} and $5^{12}6^2$ cages. Instead of the analyzed structure, the main interactions between the ionic pair and the hydrate are hydrogen bonds, where the chloride anion plays as hydrogen bond acceptor. Note that $\Delta E^{IL\text{-}cluster}$ values are increasing as a function of the number of hydrogen bonds between chloride anion and the hydrate. Structure VIII only yields one hydrogen bonds between chloride anion and the hydrate (concretely with one cage 5^{12}, while interactions with cage $5^{12}6^2$ takes places between methyl hydrogen and O atoms of the cage). Structure IX / XII leads to two / three hydrogen bonds, one of them with a cage 5^{12}, while the remaining bond are formed between the anion and cage $5^{12}6^2$. Accordingly, structures VIII, IX and VII yield one hydrogen bond between chloride anion and cage 5^{12}, while increase of $\Delta E^{IL\text{-}cluster}$ values are due to interaction between chloride anion and one cage $5^{12}6^2$. Those results agree with those obtained from structures I-IV, which pointed out to stronger interactions between ChCl and $5^{12}6^2$. In short, this second approximation has been allowed the study of the interaction mechanism in a more realistic environment. However based on interaction energies, both approximations lead to similar conclusions.

4. Conclusions

Qatari natural gas type mixture and a diluted sample of it using nitrogen have been characterized for their hydrate formation and dissociation conditions using two different experimental methods. A biocompatible ionic liquid: choline chloride at 1 and 5 wt% concentration was tested for its hydrate inhibition efficiency for both Qatari natural gas hydrates and those from diluted sample. The IL acts similar to thermodynamic inhibitor at both concentrations. However, it was not as effective as classical inhibitors. The other way of looking at this data was to consider N_2 as hydrate inhibitor itself, which was used for making the system, diluted (N_2 rich). It was found that mixing N_2 is an effective and economic way of inhibiting gas hydrates compared to chemical inhibition for the studied system. The used computational approach based on DFT allowed inferring the mechanism of interaction between the ionic liquid and model hydrate cages. The obtained results are useful and could be helpful for the Qatar oil and gas industries to plan the flow assurance strategies.

ACKNOWLEDGEMENT

This work was made possible by NPRP grant #6-330-2-140 and #5-590-2-238 from the Qatar National Research Fund (a member of Qatar Foundation). The statements made herein are solely the responsibility of the authors.

References

1. Sloan, E. D., Jr., Fundamental principles and applications of natural gas hydrates, *Nature* **2003**, *426*, **353 - 359**.
2. Kondo, W.; Ohtsuka, K.; Ohmura, R.; Takeya, S.; Mori, Y. H. Clathrate-hydrate formation from a hydrocarbon gas mixture: compositional evolution of formed hydrate during an isobaric semi-batch hydrate-froming operations. *Appl. Energy* **2014**, *113*, **864 – 871**.
3. Ludwig, R. Water: from clusters to the bulk. *Angew. Chem. Int. Ed.* **2001**, *40*, **1808 – 1828**.
4. Moon, C.; Taylor, P. C.; Rodger, P. M. Molecular dynamics study of gas hydrate formation. *J. Am. Chem. Soc*. **2003**, *125*, **4706 – 4707**.
5. Anderson, R.; Chapoy, A.; Tohidi, B. Phase relations and binary clathrate hydrate formation in the system H_2-THF-H_2O. *Langmuir* **2007**, *23*, **3440 – 3444**.
6. Mohamed, N. A. *Avoiding Gas Hydrate Problems in Qatar Oil and Gas Industry: Environmentally Friendly Solvents for Gas Hydrate Inhibition,* M. S. Thesis, Qatar University, Qatar, Nov. **2014**.
7. Giavarini, C.; Hester, K. Hydrates seen as a problem for oil and gas industry, In *Gas Hydrates: Immense energy potential and environmental challenges* **2011**, **pp 97 – 116**.
8. The world's biggest natural gas reserves (12th Nov 2013), Hydrocarbons-technology.com (retrieved on 7th April 2015).
9. Mokhatab, S.; Poe, W. A.; Speight, J. G. *Handbook of natural gas transmission and processing*; Elsevier Inc., **2006**.
10. Anderson, F. E.; Prausnitz, J. M. Inhibition of gas hydrates by methanol. *AIChE J.* **1986**, *32*, **1321 – 1333**.
11. Lafond, P. G.; Olcott, K. A.; Sloan, E. D.; Koh, C. A.; Sum, A. K. Measurements of methane hydrate equilibrium in systems inhibited with NaCl and methanol. *J. Chem. Thermodyn.* **2012**, *48*, **1 – 6**.
12. Kelland, M. A. History of the development of low dosage hydrate inhibitors, *Energy Fuels* **2006**, *20*, **825 – 847**.
13. Perfeldt, C. M.; Chua, P. C.; Daraboina, N.; Friis, D.; Kristiansen, E.; Ramlov, H.; Woodley, J. M.; Kelland, M. A.; Solms, N. V. Inhibition of gas hydrate nucleation and

growth: Efficacy of an antifreeze protein from the longhorn beetle Rhagiummordax. *Energy Fuels* **2014**, *28*, **3666 - 3672**.

14. Tariq, M.; Rooney, D.; Othman, E.; Aparicio, S.; Atilhan, M.; Khraisheh, M. Gas hydrate inhibition: a review of the role of ionic liquids, *Ind. Eng. Chem. Res.* **2014**, *53*, **17855 – 17868**.
15. Petkovic, M.; Seddon, K. R.; Rebelo, L. P. N.; Pereira, C. S. Ionic liquids: a pathway to environmental acceptability, *Chem. Soc. Rev.*, **2011**, *40*, **1383 – 1403**.
16. Zhu, Y.; Shi, B.; Fang, C. The isotopic composition of molecular nitrogen: Implications on their origins in natural gas accumulations. *Chem. Geol.* **2000**, *164*, **321 - 330**.
17. Czechowicz, D.; Skutil, K.; Taniewski, M. Nitrogen rich natural gases as a potential direct feedstock for some novel methane transformation process. Part 1: Oxidative processes, *Energy Fuels* **2009**, *23*, **4438 – 4448**.
18. Obanijesu, E. O.; Barifcani, A.; Pareek, V. K.; Tade, M. O. Experimental study on feasibility of H2 and N2 as hydrate inhibitors in natural gas pipelines, *J. Chem. Eng. Data* **2014**, *59*, **3756 – 3766**.
19. Bahadori, A. Correlation accurately predicts hydrate forming pressure of pure components, *J. Can. Pet. Technol*. **2008**, *47*, **13 – 16**.
20. Semenov, A. P.; Medvedev, V. I.; Gushchin, P. A.; Yakushev, V. S. Effect of heating rate on the accuracy of measuring equilibrium conditions for methane and argon hydrates, *Chem. Eng. Sci*. **2015**, 137, 161 – 169.
21. HYDRAFLASH® URL: http://www.hydrafact.com/index.php?page=software (last retrieved on 7th April 2015).
22. Tohidi, B.; Burgass, R. W.; Danesh, A.; Østergaard, K. K.; Todd, A. C. Improving the Accuracy of Gas Hydrate Dissociation Point Measurements. *Ann. N.Y. Acad. Sci*. **2000,** *912*, **924–931**.
23. Daraboina, N.; Malmos, C.; Solms, N. V. Synergistic kinetic inhibition of natural gas hydrate formation. *Fuel* **2013**, *108*, **749 - 757**.
24. Lone A.; Kelland, M. A. Exploring kinetic hydrate inhibitor test methods and conditions using a multicell stell rocker rig. *Energy Fuels* **2013**, *27*, **2536 – 2547**.

25. Mady, M. F.; Bak, J. M.; Lee, H.; Kelland, M. A. The first kinetic hydrate inhibition investigation on fluorinated polymers: Poly(fluoroalkylacrylamide)s. *Chem. Eng. Sci*. **2014**, *119*, **230 – 235**.
26. Wang, J.; Lu, H.; Ripmeester, J. A. Raman spectroscopy and cage occupancy of hydrogen clathrate hydrate from first-principle calculations. *J. Am. Chem. Soc.* **2009**, *131*, **14132-14133**.
27. Ramya, K. R.; Kumar, G. V. P.; Venkatnathan, A. Raman spectra of vibrational and librational modes in methane clathrate hydrates using density functional theory. *J. Chem. Phys*. **2012**, *136*, **174305**.
28. Atilhan, M.; Pala, N.; Aparicio, S. A quantum chemistry study of natural gas hydrates. *J. Mol. Mod*. **2014**, *20*, **1-15**.
29. Grimme, S. Semiempirical GGA-type density functional constructed with a long-range dispersion correction. *J. Comput. Chem.* **2006**, *27*, **1787-1799**.
30. Tang, L.; Su, Y.; Liu, Y.; Zhao, J.; Qiu, R. Nonstandard cages in the formation process of methane clathrate: Stability, structure, and spectroscopic implications from first-principles. *J. Chem. Phys*. **2012**, *136*, **224508**.
31. Ramya, K. R.; Venkatnathan, A. Stability and reactivity of methane clathrate hydrates: insights from density functional theory. *J. Phys. Chem. A* **2012**, *116*, **7742-7745**.
32. Cohen, A. J.; Mori-Sánchez, P.; Yang, W. Challenges for density functional theory. *Chem. Rev*. **2012**, *112*, **289-320**.
33. Chai, J. D.; Head-Gordon, M., Systematic optimization of long-range corrected hybrid density functionals. *J. Chem. Phys*. **2008**, *128*, **084106**.
34. Chai, J. D. ; Head-Gordon, M. Long-range corrected hybrid density functionals with damped atom-atom dispersion corrections. *Phys. Chem. Chem. Phys*. **2008**, *10*, **6615-6620**.
35. Boys, S. F.; Bernardi, F. The calculation of small molecular interactions by the differences of separate total energies. Some procedures with reduced errors. *Mol. Phys*. **1970**, *19*, **553-566**.
36. Frisch, M. J.; Trucks, G. W.; Schlegel, H. B.; Scuseria, G. E.; Robb, M. A.; Cheeseman, J. R.; Scalmani, G.; Barone, V.; Mennucci, B.; Petersson, G. A.; Nakatsuji, H.; Caricato, M.; Li, X.; Hratchian, H. P.; Izmaylov, A. F.; Bloino, J.; Zheng, G.; Sonnenberg, J. L.;

Hada, M.; Ehara, M.; Toyota, K.; Fukuda, R.; Hasegawa, J.; Ishida, M.; Nakajima, T.; Honda, Y.; Kitao, O.; Nakai, H.; Vreven, T.; Montgomery Jr., J. A.; Peralta, J. E.; Ogliaro, F. O.; Bearpark, M. J.; Heyd, J.; Brothers, E. N.; Kudin, K. N.; Staroverov, V. N.; Kobayashi, R.; Normand, J.; Raghavachari, K.; Rendell, A. P.; Burant, J. C.; Iyengar, S. S.; Tomasi, J.; Cossi, M.; Rega, N.; Millam, N. J.; Klene, M.; Knox, J. E.; Cross, J. B.; Bakken, V.; Adamo, C.; Jaramillo, J.; Gomperts, R.; Stratmann, R. E.; Yazyev, O.; Austin, A. J.; Cammi, R.; Pomelli, C.; Ochterski, J. W.; Martin, R. L.; Morokuma, K.; Zakrzewski, V. G.; Voth, G. A.; Salvador, P.; Dannenberg, J. J.; Dapprich, S.; Daniels, A. D.; Farkas, A. D. N.; Foresman, J. B.; Ortiz, J. V.; Cioslowski, J.; Fox, D. J. Gaussian 09, Gaussian, Inc.: Wallingford, CT, USA, **2009**.

37. Perdew, J. P.; Ernzerhof, K. B. Generalized gradient approximation made simple. *Phys. Rev. Lett*. **1996**, *77*, **3865**.
38. Soler, J. M.; Artacho, E.; Gale, J. D.; García, A.; Junquera, J.; Ordejón, P.; Sánchez-Portal, D. The SIESTA method for ab initio order-N materials simulation. *J. Phys. Condens. Mat*. **2002**, *14*, **2745**.
39. Lin, Y. S.; Li, G. D.; Mao, S. P.; Chai, J. D. Long-range corrected hybrid density functionals with improved dispersion corrections. *J. Chem. Theory Comput*. **2013**, *9*, **263-272**.
40. Neese, F. The ORCA program system. Wiley Interdisciplinary Reviews: *Computational Molecular Science* **2012**, *2*, **73-78**.
41. Sa, J-H.; Kwak, G-H.; Lee, B. R.; Ahn, D.; Lee, K-H. Abnormal incorporation of amino acids into the gas hydrate crystal lattice. *Phys. Chem. Chem. Phys.* **2014**, *16*, **26730 – 26734**.
42. Walker, V. K.; Zeng, H.; Ohno, H.; Daraboina, N.; Sharifi, H.; Bagherzadeh, S. A.; Alavi, S.; Englezos, P. Antifreeze proteins as gas hydrate inhibitors. *Can. J. Chem.* (doi: 10.1139/cjc-2014-0538)
43. Perrin, A.; Musa, O. M.; Steed, J. W. The chemistry of low dosage clathrate hydrate inhibitors. *Chem. Soc. Rev*. **2013**, *42*, **1996 – 2015**.
44. Kang, S-P.; Kim, E. S.; Shin, J-Y.; Kim, H-T.; Kang, J. W.; Cha, J-H.; Kim, K-S. Unusual synergy effect on methane hydrates inhibition when ionic liquid meets polymer. *RSC Adv*. **2013**, *3*, **19920 – 19923**.

45. Park, S.; Lim, D.; Seo, Y.; Lee, H. Incorporation of ammonium fluoride into clathrate hydrate lattices and its significance in inhibiting hydrate formation. *Chem. Comm.* **2015**, *51*, **8761 – 8764**.

Experimental and DFT Approach on the Determination of Natural Gas Hydrate Equilibrium with the use of Excess N_2 and Choline-Chloride Ionic Liquid as an Inhibitor

Mohammad Tariq[1ξ], Mert Atilhan[1*] and Majeda Khraisheh[1*]

Enas Othman[2ξ] and Marcelo Castier[2*]

Gregorio García[3] and Santiago Aparicio[3]

Bahman Tohidi[4]

*Corresponding authors (mert.atilhan@qu.edu.qa ; m.khraisheh@qu.edu.qa; maercelo.castier@qatar.tamu.edu)

[ξ] Equal contribution

[1]Department of Chemical Engineering, Qatar University
[2]Chemical Engineering Department, Texas A&M University at Qatar
[3]Department of Chemistry, University of Burgos, Spain
[4]Institute of Petroleum Engineering, Heriot Watt-University, United Kingdom

GRAPHICAL TOC